Sensitivity of Midlatitude Storm Intensification to Perturbations in the Sea Surface Temperature near the Gulf Stream

JAMES F. BOOTH*

Department of Atmospheric Sciences, University of Washington, Seattle, Washington

LUANNE THOMPSON

School of Oceanography, University of Washington, Seattle, Washington

JÉRÔME PATOUX

Department of Atmospheric Sciences, University of Washington, Seattle, Washington

KATHRYN A. KELLY

Applied Physics Laboratory, University of Washington, Seattle, Washington

(Manuscript received 5 August 2011, in final form 20 October 2011)

ABSTRACT

The Gulf Stream region is a primary location for midlatitude storm cyclogenesis and growth. However, the influence of sea surface temperature (SST) on storms in the region is still under question, particularly after a storm has developed. Using the Weather Research and Forecasting (WRF) model, a storm that intensified as it transited northward across the Gulf Stream is simulated multiple times using different SST boundary conditions. These experiments test the storm response to changes in both the absolute value of the SST and the meridional SST gradient. Across the different simulations, the storm strength increases monotonically with the magnitude of the SST perturbations, even when the perturbations weaken the SST gradient. The storm response to the SST perturbations is driven by the latent heat release in the storm warm conveyor belt (WCB). During the late stages of development, the surface fluxes under the storm warm sector regulate the supply of heat and moisture to the WCB. This allows the surface fluxes to govern late-stage intensification and control the storm SST sensitivity. The storm warm front also responds to the SST perturbations; however, the response is independent of that of the storm central pressure. These modeling results suggest that the SST beneath the storm can have just as important a role as the SST gradients in local forcing of the storm.

1. Introduction

The Gulf Stream region is a preferential location for midlatitude storm cyclogenesis in winter (e.g., Hoskins and Hodges 2002). The primary conditions that make the region favorable for storm formation are the atmospheric stationary wave pattern and the land–sea contrast (Brayshaw et al. 2009). However, recent literature suggests that the meridional gradient in sea surface temperature (SST) created by the Gulf Stream is also important (see Kelly et al. 2010 for review). For instance, Minobe et al. (2008) demonstrated that the Gulf Stream SST gradient affects the troposphere above it, with the frontal signature extending well above the atmospheric boundary layer in the annual mean. Nakamura et al. (2004) and Nakamura and Yamane (2009) suggest that variability in the SST gradient can cause changes in low-level atmospheric baroclinicity that force variability in the storm tracks.

Case studies of storms also show that strong, low-troposphere temperature gradients associated with the Gulf Stream aid storm formation and intensification

* Current affiliation: NASA Goddard Institute for Space Studies, Department of Applied Physics and Applied Mathematics, University of Columbia, New York, New York.

Corresponding author address: James F. Booth, NASA Goddard Institute for Space Studies, Department of Applied Physics and Applied Mathematics, University of Columbia, 200 S. W. Mudd Building, MC 4701, 500 W 120th St., New York, NY 10027.
E-mail: jfb2130@columbia.edu

DOI: 10.1175/MWR-D-11-00195.1

© 2012 American Meteorological Society

(e.g., Cione et al. 1993; Giordani and Caniaux 2001; Jacobs et al. 2007). From Florida north to Virginia, the Gulf Stream flows parallel to the coast. This creates a strong surface temperature gradient from the cold land to the warm ocean in winter. Cione et al. (1993) showed that the strength of the surface gradient was useful for forecasting the strength of storms forming in this region. Jacobs et al. (2005) improved this forecast metric by incorporating information about the approaching upper-level trough. The improvement, by means of additional information on the upper-level circulation, reinforces one of the main tenets in the theory of storm formation in this region: while the ocean surface forcing is important, the primary driver of storm intensification is the upper-level circulation.

Through mechanisms that are separate from the SST gradient, the fluxes of heat and moisture from the ocean surface can also strengthen storms, especially the fluxes that occur prior to storm onset. Kuo et al. (1991) and Reed et al. (1993b) showed that turning off the surface fluxes in a numerical model creates a much weaker storm. Kuo et al. (1991) pinpointed the 24-h period prior to storm intensification as being the time when the fluxes matter most. This warming and moistening of the air prior to storm formation is termed preconditioning. The preconditioning strengthens the storm by contributing to the latent heating in the storm warm conveyor belt (WCB; Reed et al. 1993b; Ahmadi-Givi et al. 2004).

The latent heat release in the WCB can have a strong role in storm intensification (Fantini 1990; Reed et al. 1993a,b; Stoelinga 1996; Wernli and Davies 1997; Ahmadi-Givi et al. 2004; Brennan and Lackmann 2005). The gradient in the diabatic heating along surfaces of constant absolute momentum generates positive potential vorticity (PV) in the lower troposphere that aides storm intensification (e.g., Stoelinga 1996). Ahmadi-Givi et al. (2004) studied a storm over the ocean where the PV associated with diabatic heating had a larger impact on storm intensification than the low-level PV associated with poleward warm advection (see Davis and Emanuel 1991, for more discussion on the PV associated with warm advection). The strong impact of moisture in the Ahmadi-Givi et al. (2004) case study is unique to certain storms. For that reason, Plant et al. (2003) extended the Petterssen and Smebye (1971) classification scheme to include a class of storms in which moisture has an important role in the development. The latent heating in the WCB also creates a negative PV anomaly in the upper troposphere (Pomroy and Thorpe 2000; Posselt and Martin 2004), but its influence remains a topic of open research (e.g., Stoelinga 2003).

Although the influence of preconditioning on storms is fairly well understood, there is some uncertainty regarding the influence of surface fluxes after a storm develops, when heat, moisture, and momentum fluxes, and possibly other mechanisms, can impact storm growth. Stoelinga (1996) found that a storm's strength increased when the planetary boundary layer (PBL) parameterization was turned off, because removing the PBL removed the storm damping associated with surface friction and momentum mixing in the model [see also Adamson et al. (2006); Beare (2007); Boutle et al. (2007) for more information on the role of surface friction]. However, by turning off the PBL scheme, Stoelinga (1996) also shut off the surface heat and moisture fluxes during development, leaving some question as to the relative roles of the momentum mixing, which damped the storm, versus the moisture and heat fluxes strengthening the storm. Toward this point, Reed et al. (1993b) studied a storm in which the heat and moisture fluxes continued to intensify the storm after development. The differential surface heat fluxes associated with the SST gradient may also contribute to late-stage storm development. Giordani and Caniaux (2001) ran three simulations of the same storm, one with observed SST and two more that had a spatially constant SST boundary condition, equal to either the observed SST maximum or minimum for the model domain. Using a spatially constant SST weakened the low-level baroclinic forcing of the surface fluxes, but this change did not dominate the storm response. Instead, the strongest storm occurred in the run with warm, spatially constant SST, and Giordani and Caniaux (2001) attribute this to the preconditioning. However, using such extreme SST perturbations (completely wiping out the SST gradient) made it difficult to assess the relative contributions of the fluxes under the WCB and the fluxes that affected the storm temperature fronts.

In this study, storm simulations are carried out using a set of SST perturbations, with the goal of improving the understanding of how surface fluxes influence storms during the later stages of development. We focus on the portion of the Gulf Stream that flows eastward after separating from the coastline. We also concentrate on the synoptic response, rather than the mesoscale. Previous studies show there is a mesoscale response to the SST distribution, which affects the timing and spatial distributions of the storm precipitation and surface winds (e.g., Businger et al. 2005; Brennan and Lackmann 2005; Jacobs et al. 2007). It should also be mentioned that the area surrounding the Gulf Stream is one of the primary development regions for bomb storms in the North Atlantic (Sanders and Gyakum 1980). The majority of case studies for the region have focused on bomb storms; however, our primary case study is a moderately strong storm.

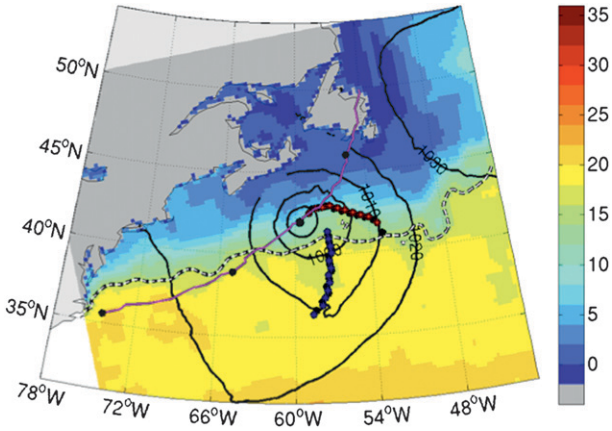

FIG. 1. The FEB2001 storm with the KF cumulus scheme with observed SST (i.e., the control simulation from experiment A1 in Table 2): shown are the storm path (magenta), as well as the SLP distribution over water (black contours) and objectively identified storm fronts at 0000 UTC 24 Feb 2001 (red dots are the warm front, blue dots are the cold front). The color shading shows the observed SST distribution, and the 15°C isotherm is highlighted (white dashed line.) The black dots along the track show the storm position every 12 h, starting at 0000 UTC 23 Feb 2001.

The paper is organized as follows. Section 2 introduces the storms used in our simulations, describes the model experiments, and defines the analysis metrics. Section 3 reports results on the SST perturbation experiments for the first modeled storm. Section 4 reports results from the second modeled storm. Section 5 contains the discussion, and section 6 is the summary.

2. Methods

Model experiments are carried out on two storms, which were selected based on their paths relative to the Gulf Stream and/or having been studied in previous experiments. The storm of major focus takes a southwest–northeast trajectory, intensifying as it crosses the Gulf Stream front (Fig. 1). This storm occurred 23–25 February 2001 and will be referred to here as FEB2001. The second storm has been the subject of previous modeling studies: the 19–21 January 1989 storm (Reed et al. 1993a,b; Kuo et al. 1996), referred to here as JAN1989. The JAN1989 took a zonal path, with the storm center moving parallel to the Gulf Stream front.

a. Model configuration

The model experiments are carried out using the Advanced Research Weather Research and Forecasting (WRF) model version 3.0 (Skamarock et al. 2008). We use 40-yr European Centre for Medium-Range Weather Forecasts (ECMWF) Re-Analysis (ERA-40; Uppala et al. 2005) for the model initial conditions and lateral boundary conditions. All of the runs are carried out without nudging. We run the simulations using 38 vertical levels, with the top level at 50 hPa. The spacing between the vertical levels increases with height, with less than 50 m between any of the lowest 10 model levels. This allows an average of eight layers within the planetary boundary layer (PBL). We use the CAM3 radiation parameterization for shortwave and longwave radiation (Kiehl et al. 1996). The cloud microphysics parameterization is the Thompson scheme (Thompson et al. 2004) and the PBL scheme is the Yonsei University scheme (YSU; Hong et al. 2006). Previous studies have shown that storms in the Gulf Stream region can be sensitive to the cumulus parameterization, due to the importance of small-scale vertical motions within the storm warm conveyor belt region (Reed et al. 1993b; Kuo et al. 1996). Therefore, some of the experiments are carried out twice: once with the Kain–Fritsch (KF) cumulus scheme (Kain and Fritsch 1993) and a second time with the Betts–Miller–Janjic (BMJ) scheme (Betts 1986; Janjic 1994).

For the FEB2001 storm, we carry out simulations using two configurations of the model: primary and supporting. In the primary configuration, the model has a 12-km grid nested inside a 36-km grid. The 12-km grid is centered over the Gulf Stream region and the 36-km grid extends 30° east and west, and 15° north and south of the storms initial and final positions. To allow a larger number of runs, the supporting experiments for the FEB2001 storm are carried out using a configuration with 36-km horizontal grid spacing only. The cumulus scheme for the supporting experiments is the Kain–Fritsch scheme, and all other parameterizations are the same as the primary experiment. For the supporting experiments, the model domain is smaller, extending only 15° east and west and 10° north and south of the final position (Table 1 summarizes the configurations). This configuration creates some limitations, which are discussed in section 2b.

To help understand the relative roles of the surface fluxes, three modified versions of the supporting configuration are created. One configuration has the surface sensible heat fluxes turned off, so that the surface moisture fluxes are the primary energy fluxes communicating the SST perturbations to the storm. A second configuration has the surface moisture fluxes turned off, leaving the sensible heat fluxes as the primary communicator. In both of these configurations, the surface friction is still active, meaning that momentum mixing within the boundary layer is also communicating the SST changes. The forcing associated with momentum mixing is not studied in isolation in this paper. One final configuration has the diabatic heating and cooling created by condensation and evaporation turned off.

TABLE 1. Model configuration of the primary and supporting experiments. Description of primary and supporting experiments.

Description of primary and supporting experiments		
	Primary expt	Supporting expt
Storms	FEB2001	FEB2001 and JAN1989
Horizontal grid spacing	12 km nested in 36 km	36 km
E–W extent of outer domain	30° beyond storm initial and final position	15° beyond storm initial and final position
N–S extent of outer domain	15° beyond storm initial and final position	10° beyond storm initial and final position
SST product	NOAA OI-SST (1/4°)	ERA-40 SST (1.125°)

b. SST boundary conditions

We create two types of SST perturbations: SST-AMP and SST-GRAD. In SST-AMP, the SST over the entire model domain is changed using a uniform perturbation. In SST-GRAD, only the SST colder than 15°C is perturbed, with the 15°C isotherm being a proxy for the temperature front of the Gulf Stream. This isotherm is used because, at the time of these two separate storms, it is where the meridional SST gradient becomes strong as one goes from south to north.

The first sets of SST-AMP perturbation experiments for the FEB2001 storm use the primary model configuration. These sets of simulations, termed SST-AMP-12km, are generated twice, once with the KF cumulus scheme and once with the BMJ scheme (A1, A2 in Table 2). A third set of SST-AMP simulations with full fluxes is carried out for the FEB2001 storm, using the supporting model configuration (B1 in Table 2). Three additional sets of simulations are also generated, all using the SST-AMP type of perturbations and the modified, supporting configurations: no sensible heat fluxes (B2), no moisture fluxes (B3), and no latent heating (B4). The SST-GRAD perturbation experiments for the FEB2001 storm are carried using the primary model configuration. These sets of simulations, termed SST-GRAD-12km, are also generated twice, using each cumulus scheme (A3, A4 in Table 2).

TABLE 2. Description of the SST perturbations for the difference sets of simulations. SST-AMP experiments have a spatially uniform SST perturbation applied to the entire model domain. SST-GRAD experiments have a spatially uniform perturbation applied to the SST that is colder that 15°C. In the experiment names in the first column, CU is shorthand for cumulus scheme, KF is Kain–Fritsch, and BMJ is Betts–Miller–Janjic. SST perturbations for each set of simulations.

SST perturbations for each set of simulations				
Experiment label/ descriptive name	SST perturbations (°C)	Method of adding SST perturbations	Starting time and duration of expt	Cumulus parameterization scheme
Primary expts: FEB2001 storm				
A1/SST-AMP-12km, CU = KF	−3.6, −1.8, −0.9, 0, +0.9, +1.8, +3.6	Gradual adjustment of perturbation	1200 UTC 22 Feb 2001 and 60-h duration	Kain–Fritsch
A2/SST-AMP-12km, CU = BMJ				Betts–Miller–Janjic
A3/SST-GRAD-12km, CU = KF	−1.8, 0, +1.8			Kain–Fritsch
A4/SST-GRAD-12km, CU = BMJ				Betts–Miller–Janjic
Supporting expts: FEB2001 storm				
B1/SST-AMP-36km, full fluxes	Ranging from −4 to +4, using increments of 0.2	Add perturbation to initial conditions	1800 UTC 22 Feb 2001 and 54-h duration	Kain–Fritsch
B2/SST-AMP-36km, no surface sensible heat flux				
B3/SST-AMP-36km, no surface moisture flux				
B4/SST-AMP-36km, no latent heating, both surface fluxes on				
Supporting expts: JAN1989 storm				
C1/SST-AMP-J89, full fluxes	Ranging from −4 to +4, using increments of 0.2	Add perturbation to initial conditions	1800 UTC 18 Jan 1989 and 66-h duration	Kain–Fritsch
C2/SST-AMP-J89, no surface sensible heat flux				
C3/SST-AMP-J89, no surface moisture flux				
C4/SST-GRAD-J89	−4 to +4, using increments of 0.4			

For the JAN1989 storm, there are three experiments with SST-AMP style perturbations: one with full physics (C1, in Table 2), another with no sensible heat fluxes (C2) and one with no moisture fluxes (C3). We also create a set of simulations for the JAN1989 storm with perturbations only applied to the SST north of the 15° isotherm: SST-GRAD-J89 (C4 in Table 2). All of the experiments for the JAN1989 storm use the model configuration of the supporting experiments.

We introduce the SST perturbations in the primary experiments in a manner that limits the initial shock of the perturbations. The SST-AMP-12km and SST-GRAD-12km simulations begin on 1200 UTC 22 February 2001, 12 h before the storm formed. During the first 6 h of the run, all of the simulations use the observed SST. Then, during the subsequent 6 h of the simulation, 1800 UTC 22 February to 0000 UTC 23 February, the SST is updated hourly using a field that has been created by interpolating linearly in time between the observed SST and the final perturbed state (see the appendix for details on the spinup). Then the SST is held fixed during the 48 h of storm growth. The SST product used for the primary experiments is the National Oceanic and Atmospheric Administration (NOAA) optimum interpolation SST (OI-SST; Reynolds et al. 2002). This SST product has 0.25° horizontal grid spacing and is available daily.

For the experiments that use the supporting configuration, the SST perturbation is introduced in a less elegant fashion. The simulations are started 6 h prior to storm formation with the SST perturbations applied at the start of the simulations and held fixed throughout the runs (see Table 2). Thus, the supporting experiments for the FEB2001 storm begin on 1800 UTC 22 February 2001. After storm formation, the simulations run for 48 h, making the total duration 54 h. All of the JAN1989 simulations begin on 1800 UTC 18 January 1989. The JAN1989 simulations run for 60 h following storm formation, making the total duration of the simulations 66 h. The experiments with the supporting configuration use the ERA-40 SST, which has 1.125° horizontal grid spacing. After November 1981, the SST used in generating ERA-40 is the 7-day-averaged Reynolds SST (Reynolds and Smith 1995).

Using time-invariant SST during the storm life cycle is justified by the fact that gridded SST products rely on satellite data that are generated from running averages over several days. This makes the true temporal resolution for these products between 24 and 48 h. Additionally, Jung and Vitart (2006) showed that a time-evolving SST does not have a significant impact on synoptic conditions for weather forecasts of 2–4 days. Jacobs et al. (2007) show that the time averaging of the SST does affect mesoscale circulation patterns; therefore, we do not focus on the mesoscale response.

The coarse SST resolution, short spinup time, and coarse horizontal grid spacing used for the supporting configuration are limitations. With coarse resolution, the influence of the SST gradient on the atmosphere is not resolved completely. There is also the possibility that, with lower resolution, the storm is responding to SST perturbations primarily through the actions of the model parameterizations. As a result, there were differences in the SST sensitivity during the earliest stages of the FEB2001 storm's life cycle (discussed further in section 3a). However, after the first 12 h of the simulation, the storm response to SST perturbations is similar for the 12- and 36-km experiments, suggesting that the 36-km runs capture the fundamental response of the synoptic system to changes in SST and surface fluxes. Additionally, the supporting configuration allows us to generate a larger number of model runs. For example, there are 41 simulations in the SST-AMP-36km set versus 7 simulations in the SST-AMP-12km set. The larger sets provide results from a greater array of SST perturbations, which helps test the robustness of the storm response.

c. *Analysis metrics*

We developed a set of analysis metrics to compare the response of the storm for the different SST configurations. The metrics are calculated relative to the position of the storm center, therefore the time axis in the figures begins when the observed storm formed: 0000 UTC 23 February for the FEB2001 storm, and 0000 UTC 19 January for the JAN1989 storm. Details of the simulation behavior prior to storm formation are discussed in the appendix.

Using hourly snapshots from the model, the sea level pressure (SLP) minimum on the lowest model level is objectively identified as the storm center. The algorithm finds the minimum after the surface pressure has been smoothed using a running average over a region with a 5-gridpoint radius. For the supporting configuration, a 3-gridpoint radius is used for the averaging. The pressure value and position of the storm center are saved for further analysis. The area-averaged surface wind speed and precipitation following the storm center (using a 10° radius around the center) are examined as additional metrics of storm strength, but we focus on the SLP minimum.

To compare the influence of latent heat release across the different simulations, we tabulate the total latent heating within the WCB. We define the total latent heating as

$$Q_{\mathrm{VOL}}(t) = \int_{\mathrm{Surface}}^{\mathrm{Model_{TOP}}} \left[\int_{\mathrm{WCB}_A(Z)} Q(x,y,z,t)\, dA \right] dz, \quad (1)$$

where Q is the model generated heating (or cooling) due to condensation. The $\mathrm{WCB}_A(Z)$ is the warm conveyor belt region at height Z, defined as the area in which the upward vertical velocity is in the strongest 95th percentile, following Sinclair et al. (2008) and Boutle et al. (2011). Since there are strong vertical winds associated with other storms within the model domain, we only use the vertical velocity within a 10° radius of the storm center to define $\mathrm{WCB}_A(Z)$. Our definition for $\mathrm{WCB}_A(Z)$ captures the forward tilt in the storm WCB (e.g., the middle panel in Fig. 2b). Both the storm radius and the vertical velocity cutoff percentile are subjective parameters, and we describe the sensitivity of Q_{VOL} to these parameters in sections 3a and 3b.

We identify the storm warm and cold fronts by applying the front detection algorithm of Hewson (1998) to the potential temperature θ on the model level that sits between 500–580 m. We also applied the method to θ on the 925-hPa surface and similar results were found (not shown). Essentially, the Hewson (1998) method determines the most likely location of fronts using threshold values for the strength of the temperature gradient ($|\nabla\theta|$), and the spatial rate of change of the length of the gradient [$\nabla(|\nabla\theta|)$]. Then, in the regions that pass the threshold test, the divergence of $\nabla(|\nabla\theta|)$ is calculated in a coordinate system rotated with the streamlines of the temperature gradient field (i.e., the along-gradient divergence). The fronts are identified as the locations in which the along-gradient divergence is equal to zero, and the cold and warm fronts are designated based on the geostrophic temperature advection at the front (in Hewson 1998, see section 6.3 for exact details of the method). An example of the objectively identified fronts is shown in Fig. 1. After identifying the fronts, we define the warm front strength as

$$\mathrm{STRENGTH_{WF}} = \frac{1}{A_{\mathrm{WF}}} \int_{A_{\mathrm{WF}}} |\nabla\theta|\, dA. \quad (2)$$

The warm frontal area, A_{WF}, is defined as the region starting at the WF and extending 2° poleward.

The area-average surface sensible heat fluxes (SHFX) that occur beneath the storm warm sector are defined using

$$\mathrm{SHFX_{WS}} = \frac{1}{A_{\mathrm{WS}}} \int_{A_{\mathrm{WS}}} \mathrm{SHFX}\, dA. \quad (3)$$

The warm sector area A_{WS} is defined as the region between the storm warm and cold fronts, within a 10° radius of the storm center. We define an analog to (3) for

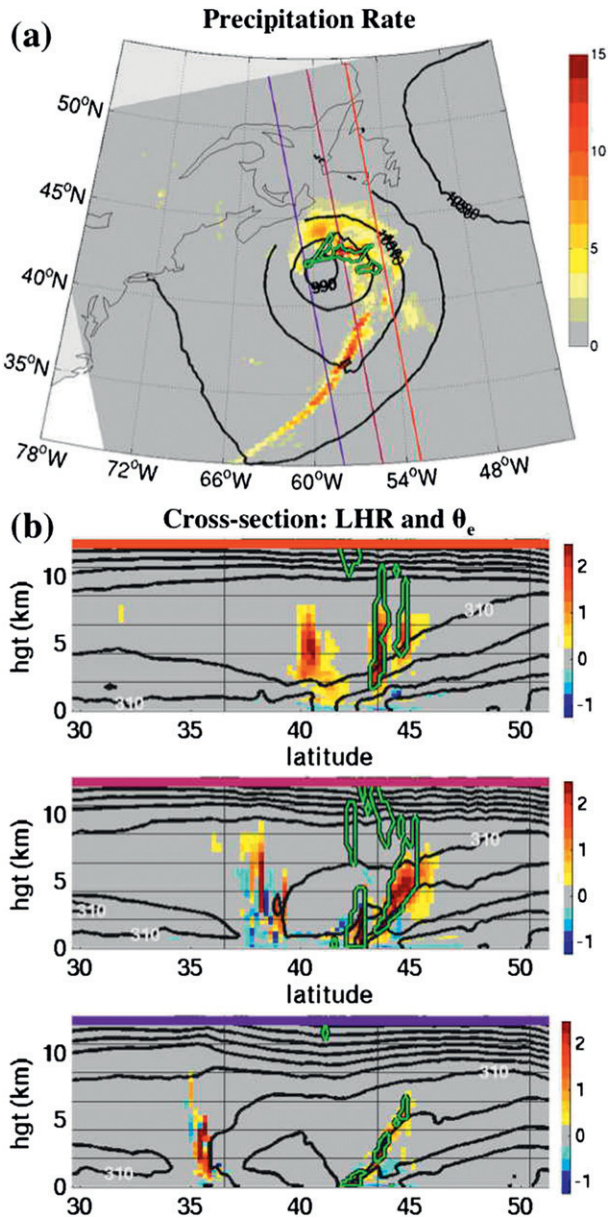

FIG. 2. Example of the WCB mask for the storm shown in Fig. 1, at the same time, 0000 UTC 23 Feb. (a) Map view of the total precipitation rate (mm h^{-1}). The green contour shows the outline of the WCB at the top of the boundary layer [$\mathrm{WCB}_A(Z)$, section 2c]. The black contours show the SLP. (b) The diabatic heating associated with condensation (color shading, K s^{-1}), and the equivalent potential temperature (black contours). The purple, maroon, and red lines mark the cross-section location for the cross sections shown in (b). The color at the top of each is associated with the lines in (a), showing the location of the cross section. The green contour outlines the location of the warm conveyor belt used in the Q_{VOL} calculation (section 2c).

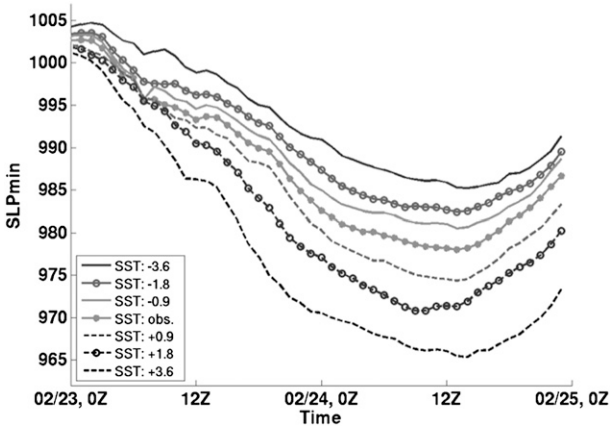

FIG. 3. The FEB2001 storm strength in SST-AMP-12km set of simulations with the KF cumulus scheme (A1 in Table 2): shown is the time evolution of the SLP minimum for the simulations, beginning at the time when the storm center is first identified in the control simulation. The solid, light gray line with solid circles is the control simulation. The three lines with SLP minima greater than the control simulation are the runs with SST perturbations of −0.9°, −1.8°, and −3.6°C, with the strongest cold perturbation corresponding to the dark, solid line. The three lines with SLP minima deeper than the control simulation are the simulations with SST perturbations of +0.9°, +1.8°, and +3.6°C, with the strongest warm perturbation corresponding to the dark, dashed line.

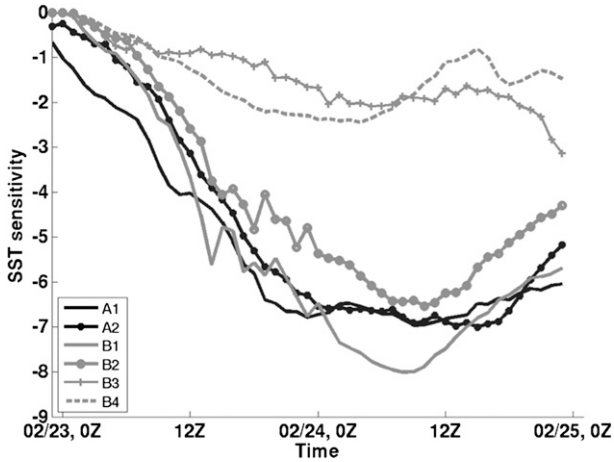

FIG. 4. The FEB2001 storm strength sensitivity $d\mathrm{SLP}(t)/d\mathrm{SST}$ as defined in (4): shown are the SST-AMP-12km experiments with the KF cumulus scheme (solid black line; experiment A1 in Table 2) and the BMJ cumulus scheme (solid black line with circles; A2), as well as, the SST-AMP-36km set of simulations with full fluxes (solid gray; B1), with no surface sensible heat flux (solid gray line with circles; B2), with no surface moisture fluxes (gray line with X marks; B3), and with no latent heat release (dashed gray line; B4).

the surface latent heat flux $\mathrm{LHFX_{WS}}$. Note that the surface latent heat flux can be converted into a moisture flux using the latent heat of vaporization. To allow a direct comparison with the sensible heat flux, we use the latent heat flux in this tabulation. But, we use the terminology ''moisture flux'' in our discussion, to help keep the surface latent heat flux separate from the latent heating within the storm.

We define $\mathrm{PBLH_{UN}}$ as the area-average of the planetary boundary layer height (PBLH) in the region under the storm, exclusive of the storm warm sector (since the PBL in the region of the storm warm sector is typically stable). We again use the 10° storm-centered radius, but mask out the region designated as the warm sector. We use the $\mathrm{PBLH_{UN}}$ as a proxy for the amount of momentum mixing occurring under the storm (e.g., Vukovich et al. 1991).

3. Results: FEB2001 case study

a. *Storm sensitivity to SST perturbations of the whole domain*

The first experiment we analyze is the SST-AMP-12km set of simulations with the KF cumulus scheme (A1 in Table 2). The SLP minima for the simulations in experiment A1 show that the storm responds monotonically to the SST changes: warmer perturbations lead to stronger storms, while cooler perturbations lead to weaker storms (Fig. 3). We find consistent results using other metrics, such as the area-averaged wind speed or precipitation in the vicinity of the storm center (not shown).

We define the sensitivity of the SLP to the SST perturbations as

$$d\mathrm{SLP}(t)/d\mathrm{SST} = \frac{\sum_{i=1}^{N} \mathrm{SST}_i' \mathrm{SLP}_i'(t)}{\sqrt{\sum_{i=1}^{N} (\mathrm{SST}_i')^2}}. \tag{4}$$

The prime indicates the deviation from the mean for a given set of simulations (calculated at each analysis time). The formulation of sensitivity [(4)] is also the sensitivity metric used in ensemble forecasting analysis (e.g., Hakim and Torn 2008). We use it here to compare the SLP response across the different sets of simulations. Note that a more negative value for (4) corresponds to a stronger sensitivity, since a lower SLP is associated with a stronger storm.

A comparison of $d\mathrm{SLP}(t)/d\mathrm{SST}$ for the different FEB2001 SST-AMP experiments with full fluxes (A1, B1, and A2) shows that the storm's response depends on the model configuration, but the differences are never that large (Fig. 4). For the KF cumulus scheme, the 12-km set of simulations (A1 in Table 2; the solid black line Fig. 4) and the 36-km set with full-fluxes (B1; the

solid gray line in Fig. 4) agree in storm sensitivity after 1200 UTC 23 February. The agreement suggests that after the first 12 h of intensification, the resolved vertical motions within the storm's warm conveyor belt become large enough to affect the central pressure minimum in the coarse resolution model. During the first 12 h of the storm, 0000–1200 UTC 23 February, the sensitivity is greater in the set of simulations with 12-km grid spacing, compared to those with 36-km grid spacing. The earlier response is created by shallow cumulus activity and resolved vertical motions at the eastern edge of the storm's genesis region in the 12-km simulations (not shown). For the two SST-AMP-12km experiments with different cumulus schemes (A1 and A2; the solid black line and the black line with circles in Fig. 4), the sensitivities differ during the first 12 h of the storm, and then converge by 0000 UTC 24 February. The difference in the initial response is associated with the behavior of the cumulus schemes and will be discussed in section 5.

The largest differences in $d\mathrm{SLP}(t)/d\mathrm{SST}$ in the FEB2001 SST-AMP experiments are connected to changes in moisture forcing (Fig. 4). The storm strength sensitivity for the experiment with no sensible heat fluxes (B2 in Table 2; the gray line with circles in Fig. 4) is very similar to the full-flux cases (A1, B1, and A2), while the sets of simulations with surface moisture flux off (B3; the gray line with Xs in Fig. 4) and with no latent heat release (B4; the gray dashed line in Fig. 4) both have a weaker sensitivity. Since these experiments, B3 and B4, have the weakest response, we conclude that latent heat release, which is tied to the SST perturbation via the surface moisture fluxes, plays a key role in the storm response to the SST changes.

The SST sensitivity of the volume-integrated latent heat release, Q_{VOL} defined in (1), also suggests that the latent heating in the WCB is the mechanism through which the SST affects the storm strength. For the SST-AMP-12km experiment with the KF scheme (A1), the time evolution for Q_{VOL} (Fig. 5) shows a monotonic increase in latent heating with the SST perturbation. The change in heating with SST, $dQ_{\mathrm{VOL}}(t)/d\mathrm{SST}$, defined by replacing SLP by Q_{VOL} in (4), is positive for the 12-km grid spacing with either cumulus scheme (A1 and A2), as well as the 36-km set of simulations (B1) (not shown). The sensitivity, $dQ_{\mathrm{VOL}}(t)/d\mathrm{SST}$, remains positive for a wide range of values of the storm radius and vertical velocity cutoff parameters used in the definition of Q_{VOL} (not shown). The response of Q_{VOL} is consistent with previous studies of the sensitivity of storms to latent heating (e.g., Reed et al. 1993b). We conclude that Q_{VOL} captures the diabatic heating component of the WCB that is responsible for providing secondary intensification to the storms.

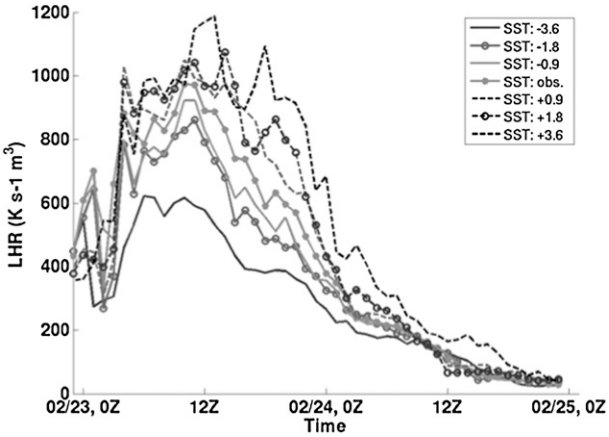

FIG. 5. The FEB2001 Q_{VOL} for the SST-AMP-12km set of simulations with the KF cumulus scheme (experiment A1 in Table 2): shown is the time evolution of the latent heat release integrated over the storm warm sector Q_{VOL} as defined by (1). The line styles are the same as in Fig. 3: the solid gray with solid circles is the control storm, the solid black line is the run with the coldest SST perturbation, and the dashed black line is the run with the warmest perturbation.

The storm path is relatively insensitive to the sign and strength of the SST perturbation in the SST-AMP experiments, for both grid spacing configurations (A1 and B1). When the tracks do diverge in experiment A1, near 1200 UTC 24 February, the stronger storms take a more northwestward path (not shown). We hypothesize that the path change reflects the increase in the cyclonic vorticity of these stronger storms, which acts to increase the northwestward propagation.

b. Storm sensitivity to SST gradient

In this subsection, we investigate the storm strength sensitivity to the gradient in SST. For these experiments, the SST on the cold side of the 15°C isotherm is warmed or cooled, effectively changing the strength of the SST gradient (discussed in section 2b). We show results for the SST-GRAD-12km sets of simulations with the KF cumulus scheme (experiment A3 in Table 2) and the BMJ scheme (A4). For both experiments, A3 and A4, we run three simulations: 1) the control, using the observed SST, 2) "cold SST-1.8" (i.e., subtracting a perturbation from the SST $<$ 15°C, which strengthens the SST gradient), and 3) "cold SST+1.8" (i.e., adding a perturbation to the SST $<$ 15°C, which weakens the gradient).

For the SST-GRAD-12km experiments, the storm strength responds more to the temperature of the SST perturbation, than to the strength of the SST gradient (Figs. 6a,b). For both sets of simulations, A3 and A4, the lowest SLP occurs in the case with the positive perturbation (the dashed lines in Figs. 6a,b), and that is the

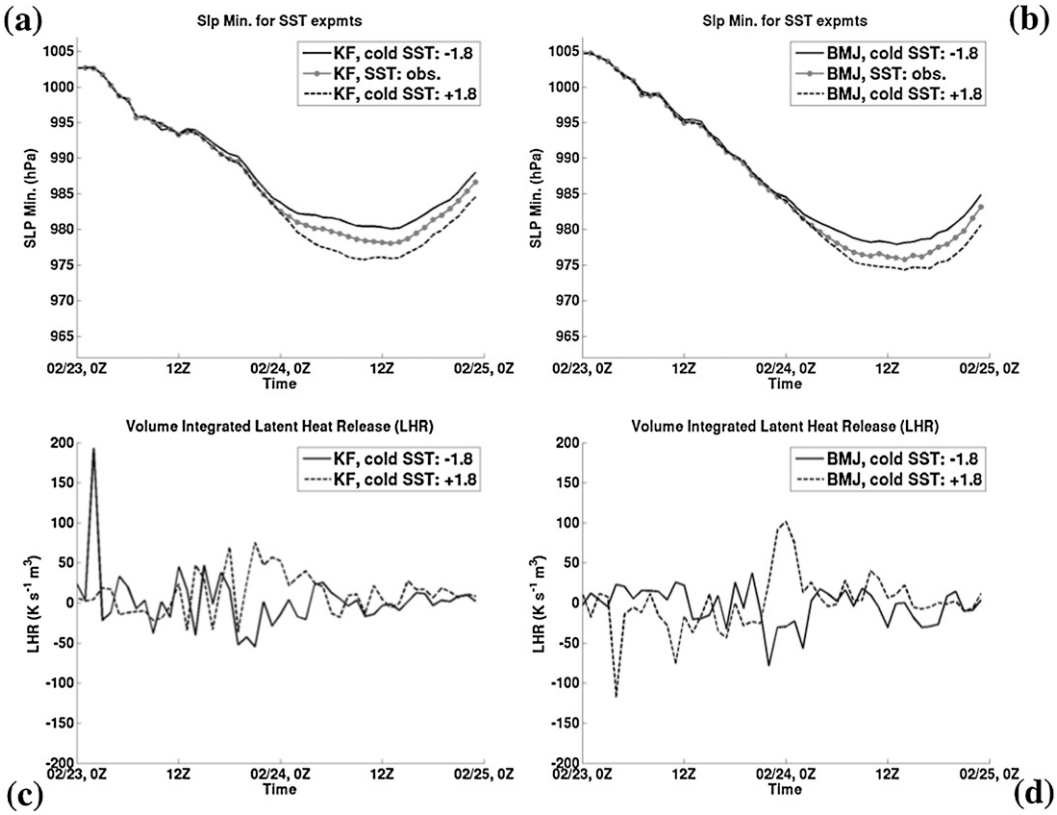

FIG. 6. The FEB2001 SLP_{MIN} and Q_{VOL} for the SST-GRAD-12km set of simulations (experiments A3 and A4 in Table 2): shown are the time evolution of the SLP minimum for (a) the set using the KF cumulus convection scheme (A3) and (b) the set using the BMJ scheme (A4). The time evolution of the differences in the latent heat release in the storm warm sector Q_{VOL} between the perturbed SST experiments and the control experiment (i.e., perturbed minus control), for the sets of experiments using the (c) KF scheme (A3) and (d) BMJ scheme (A4). In (a) and (b), the gray line with circles is this control experiment. In (a)–(d), the dashed lines show the simulations with a positive SST perturbation and the solid, dark lines show the simulations with the negative SST perturbation. The time evolution of Q_{VOL} for the control experiment is shown in Fig. 5.

perturbation that creates the weakest SST gradient. Conversely, when the negative perturbation is applied to the region north of the 15°C contour, the storm is weakest (the dark solid lines in Figs. 6a,b), despite the stronger meridional SST gradient. The dependence of storm strength on the SST perturbation, rather than the SST gradient, also holds for the area-averaged wind speed and precipitation metrics (not shown).

For the simulations with SST perturbations, in both of the SST-GRAD-12km experiments (A3 and A4), the change in the condensational heating in the WCB, Q_{VOL} from (1), has the same sign as the SST perturbation (Figs. 6c,d). Beginning near 0000 UTC 24 February, Q_{VOL} is greatest in the simulation with the positive SST perturbation (the dashed line in Figs. 6c,d). Since this simulation had the deepest SLP minima, the Q_{VOL} result suggests that the positive SST perturbation increased the latent heat release, which intensified the storm. Similarly, at 0000 UTC 24 February, Q_{VOL} is weakest in the simulation with a negative SST perturbation (solid line in Figs. 6a,b). The timing of the divergence in storm strength (Figs. 6a,b), within either set of simulations (A3 or A4), occurs when the majority of the storm warm sector has moved north of the 15°C SST isotherm, placing the base of the warm sector over the perturbed SSTs (Fig. 1).

A tabulation of the surface fluxes into the storm warm sector for the SST-GRAD-12km experiment with the KF scheme (A3) shows that the heat and moisture fluxes vary consistently with the storm strength. Between 1800 UTC 23 February and 0600 UTC 24 February, the simulation with the positive SST perturbation has the largest latent heat flux into its warm sector (dashed line Fig. 7a). In all of the simulations, the sensible heating $SHFX_{WS}$ becomes negative as the storm warm sector moves north (0000 UTC 24 February in Fig. 7b). The

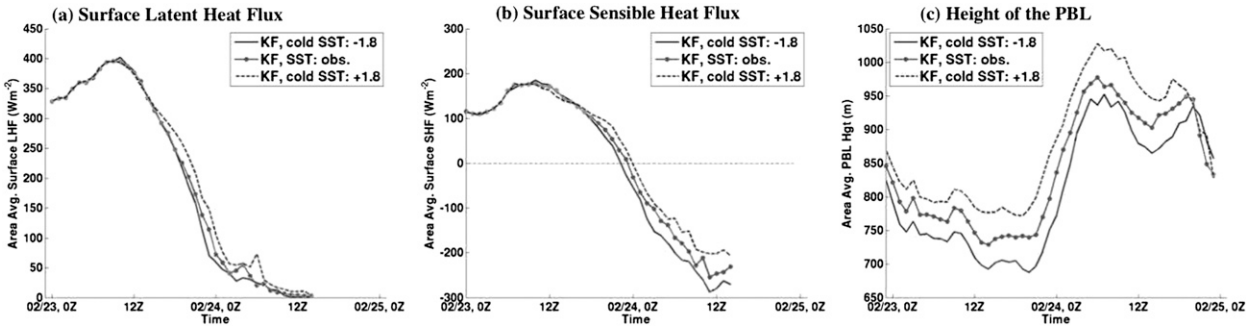

FIG. 7. Surface forcing following the storm in the SST-GRAD-12km set of simulations with the KF cumulus scheme (experiment A3 in Table 2): (a) the area-average of the surface latent heat flux $LHFX_{WS}$; (b) surface sensible heat flux $SHFX_{WS}$ from (3), under the storm warm sector; and (c) the area average of the PBL height under the storm, exclusive of the warm sector, $PBLH_{UN}$. Late in the storm life cycle, $LHFX_{WS}$ and $SHFX_{WS}$ become difficult to calculate, because the warm sector moves over land, so the time series end at 1500 UTC 24 Feb. In (a)–(c), the gray line with circles shows the control simulation, the dashed line shows the simulation with the positive SST perturbation, and the dark solid line shows the simulation with the negative SST perturbation.

heat loss lowers both the buoyancy and the saturation vapor pressure of the air at the base of the WCB. The amplitude of the surface heat loss changes with the SST perturbations and the run with a positive SST perturbation has the smallest heat loss (dashed line Fig. 7b). This likely contributes to the storm reaching a deeper SLP minimum.

The vertical momentum fluxes in the PBL, which can damp the storm, increase monotonically with the SST perturbations (Fig. 7c). For the simulations in experiment A3, the area average of the height of the PBL ($PBLH_{UN}$ from section 2c) shows that the storm with the positive SST perturbation has the deepest PBL (the dashed line in Fig. 7c). This suggests that the positive perturbation helps generate more momentum mixing, which makes sense because warmer SSTs can increase the boundary layer instability. However, the storm damping associated with the increased PBL activity is overwhelmed by the storm intensification associated with the additional moisture fluxed into, as well as the weaker sensible heat loss out of, the storm warm sector.

The response of the storm warm front reflects the changes in the SST gradient (Fig. 8). Applying the $STRENGTH_{WF}$ metric defined in (2) to the simulations in experiment A3, we find that the storm warm front is strongest for the simulation that has the negative SST perturbation (the dark, solid line in Fig. 8). Thus, the stronger SST gradient strengthens the storm's surface warm front. However, the response of the warm front is opposite that of the SLP minimum. Additionally, the storm warm front responds to the SST perturbation earlier than the storm central pressure: $STRENGTH_{WF}$ diverges in the experiment A3 simulations at 1800 UTC 22 February (see the appendix for details on the behavior during spinup).

4. Results: JAN1989 case study

We now turn our attention to a storm that was previously studied by Reed et al. (1993a,b) and Kuo et al. (1996), which traveled parallel to the Gulf Stream, rather than across it. Our control experiment, with observed SST, reproduces the results of Reed et al. (1993b) in path and SLP distribution (Fig. 9a). In addition, the time evolution of the storm SLP minimum matches that found in Reed et al. with a strong intensification occurring during the 12-h period beginning at 1200 UTC 19 January (Fig. 9b and Fig. 3 in Reed et al. 1993b).

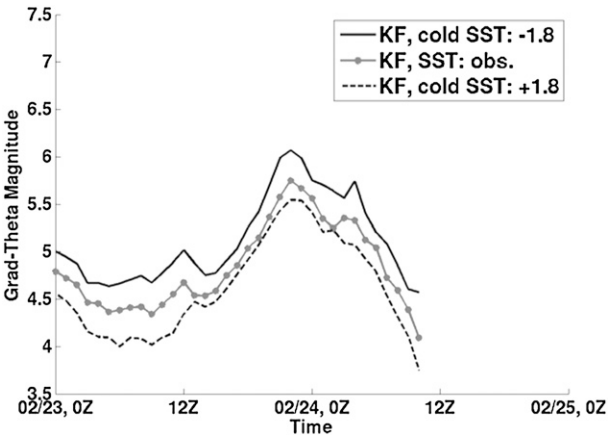

FIG. 8. The $STRENGTH_{WF}$ in the SST-GRAD-12km set of simulations with the KF cumulus scheme (experiment A3 in Table 2): the time evolution of the strength of the storm warm front, $STRENGTH_{WF}$ from (2). After 1200 UTC 24 Feb, the warm front moves over land and the metric is complicated by the topography of Newfoundland, so it is omitted here. The gray line with circles shows the control simulation, the dashed line shows the simulation with the positive SST perturbation, and the dark solid line shows the simulation with the negative SST perturbation.

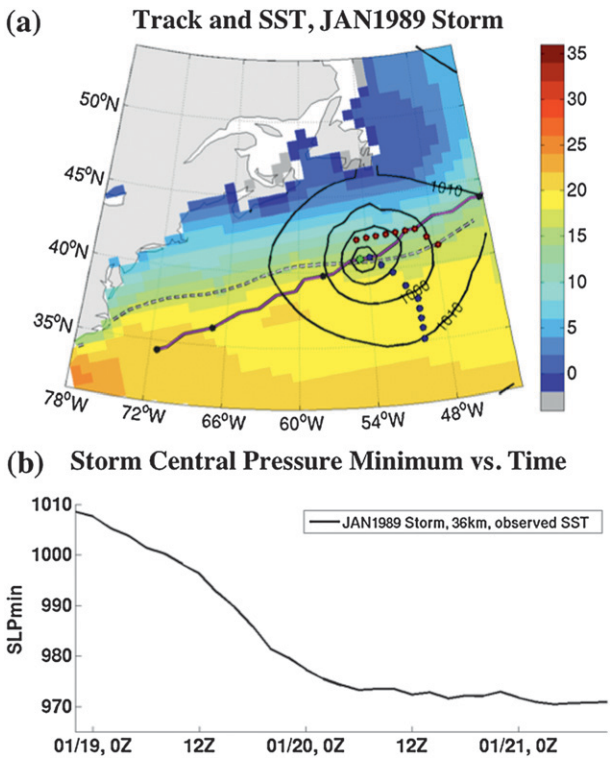

FIG. 9. The JAN1989 storm path and SLP time evolution for the control simulation with observed SST: (a) the storm path (magenta), and the SLP distribution (black contours) and objectively identified storm fronts (red dots are the warm front, blue dots are the cold front) at 0600 UTC 20 Jan 1989. The color shading shows the observed SST distribution and the 15°C isotherm is highlighted (white dashed line). The black dots along the track show the position of the storm every 12 h, beginning at 0000 UTC 19 Jan. The last black dot is at 0000 UTC 21 Jan, and the black dot for 1200 UTC 20 Jan is hidden under the warm front. (b) Time evolution of the SLP minimum for the storm in the simulation with observed SST.

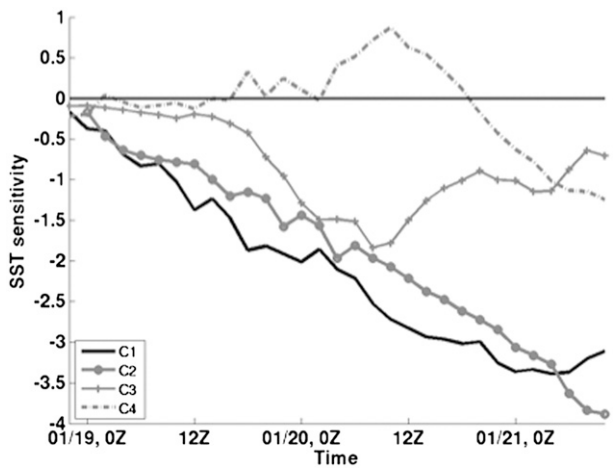

FIG. 10. The JAN1989 storm strength sensitivity $d\mathrm{SLP}(t)/d\mathrm{SST}$ from (4). The sets of simulations shown are the SST-AMP-J89 with full fluxes (dark gray line; experiment C1 in Table 2), no sensible heat flux (gray with circles; C2), no moisture flux simulation (gray with Xs; C3), and the SST-GRAD-J89 set of simulations (dashed–dotted gray line; C4).

The storm strength sensitivity to SST, $d\mathrm{SLP}(t)/d\mathrm{SST}$ from (4), for the JAN1989 storm is predominantly driven by the surface moisture fluxes (Fig. 10). For the full-fluxes and no sensible heat flux experiments (C1 and C2 in Table 2), the $d\mathrm{SLP}(t)/d\mathrm{SST}$ is similar for the entire simulation (dark gray line and light gray line with circles in Fig. 10, respectively). The sensitivity agreement for these two sets reinforces the importance of the surface moisture fluxes for the storm response to SST. The $d\mathrm{SLP}(t)/d\mathrm{SST}$ for the no-moisture flux experiment (C3; solid gray line with Xs in Fig. 10) has a magnitude comparable to the full-fluxes case (C1) from 0000 UTC 20 January until 1200 UTC 20 January. Later in the storm life cycle, the sensitivity weakens in the no moisture flux set (C3), while the sensitivity continues to grow in the full-flux (C1) and no sensible heat flux (C2) sets of simulations (Fig. 10). These results suggest that 1) the sensible heat fluxes were nearly as important as the moisture fluxes during the first 24 h of development for the JAN1989 storm, and 2) late in the storm development, the moisture fluxes were the controlling factor.

The sensitivity, $d\mathrm{SLP}(t)/d\mathrm{SST}$, for the SST-GRAD-J89 set of simulations (C4 in Table 2) shows that perturbations to the SST gradient can have a local impact on the storm strength (dashed gray line in Fig. 10). The sensitivity for SST-GRAD-J89 is positive from 0300 to 1800 UTC 20 January. When $d\mathrm{SLP}(t)/d\mathrm{SST} > 0$, the runs with the negative SST perturbations, and hence a stronger SST gradient, are stronger. By 1800 UTC 20 January, $d\mathrm{SLP}(t)/d\mathrm{SST}$ is negative, meaning that the storms in the simulations with positive SST perturbations are stronger, despite there being a weaker SST gradient. By this time, most of the JAN1989 storm's warm sector is north of the 15°C isotherm, placing the base of the WCB over the perturbed SSTs (see Fig. 9a as a reference). Thus, it appears that strengthening the SST gradient can strengthen the storm, but only if the SST perturbations that affect the SST gradient do not also cause changes in the surface fluxes under the storm warm sector.

Our results can be used to explain one of the experiments in Reed et al. (1993b). Their study included one storm simulation with the entire SST field in the Gulf Stream region shifted northwest by 3° of latitude, and a second simulation with a similar shift of the SST southeast. For the northwest shift, the storm strength did not change compared to the control SST, but for the southwest shift the storm weakened. Based on our

finding that the storm responds strongly to the forcing associated with the moisture fluxes into the storm warm sector, the asymmetry in the response for the two experiments appears to relate to the spatial distribution of the SST gradient in the Gulf Stream region. South of the Gulf Stream, the meridional SST gradient is very weak, so shifting the SST northwest barely changed the absolute temperatures under the JAN1989 storm's warm sector. As a result, the storm strength did not change in that simulation. North of the Gulf Stream, the SST gradient is strong, with the temperatures decreasing significantly from the Gulf Stream to the coast. So, the shift of the SST southwest placed much colder water under the storm warm sector and led to a weaker storm.

5. Discussion

For both of the storms investigated, the surface heat and moisture fluxes under the storm warm sector appear to control the surface forcing of storm strength during the late stages of development. For the experiments in which the entire SST field is uniformly perturbed (SST-AMP) and for those in which only the SST north of the Gulf Stream is perturbed (SST-GRAD), the storm strength changes monotonically with the SST: warmer perturbations create stronger storms. Furthermore, the response of the storm strength to the perturbations in the SST-GRAD-12km experiments (A3 and A4 in Table 2) does not occur until the storm warm sector has moved over the region of perturbed SST.

We theorize that, in the late phases of storm development, the surface fluxes of heat and moisture beneath the storm warm sector govern the storm strength. We choose the term "govern" to emphasize that these fluxes regulate, rather than supply, the heat and moisture that reach the WCB. This distinction is important because it calls attention to the difference between the behavior reported here and the preconditioning that occurs prior to storm formation. Preconditioning in the sense described in Reed et al. (1993b) occurs when cold air blows over warm water creating an unstable atmospheric boundary layer and large fluxes of heat and moisture (summarized recently in Shaman et al. 2010). The late stage fluxes highlighted in this paper occur beneath the storm warm sector, after the storm has formed. In this case, the boundary layer is stable due to the warm advection (or weakly unstable), and the fluxes of moisture and heat from ocean to atmosphere are small or negative. However, the fluxes impact the strength of the storm through their influence on the latent heat release in the WCB, which in turn can impact the storm dynamics.

The fluxes that occur in the wake of a storm can have nonlocal impacts by affecting a subsequent storm in the region, while the fluxes into the warm sector that we study here have a local impact. This is an important qualifier on our study's results: by design we can only study the local impacts of the surface fluxes. It is also worth mentioning that the heat and moisture fluxes that occur ahead of the warm sector can influence the moisture supply to the WCB (Boutle et al. 2010). In our experiments, this influence was secondary to the role of the fluxes directly beneath the warm sector, as evidenced by the timing of the storm sensitivity in the SST-GRAD-12km experiments (Figs. 6a,b; A3 and A4 in Table 2).

The response of the storm warm front to the SST perturbations shows that SST can be important to storm frontal strength, although the frontal strength may not necessarily feed back on the strength of the storm. In the SST-GRAD-12km experiments (A3 and A4), $\mathrm{STRENGTH_{WF}}$ increased with stronger SST gradient perturbations, indicating a modification of the storm fronts by the surface fluxes. However, the storm central pressure minimum did not respond to these changes. [This is consistent with the storm's temperature fronts being a reflection of the storm circulation rather than a cause (e.g., Martin 2006, 187–234)]. Our results suggest two important points: 1) an oceanic storm's frontal strength depends on both the temperature advection associated with the storm and the surface fluxes local to the front; and 2) during the late stages of storm intensification, the SST influence on storm temperature fronts is not as important as the SST influence on moisture availability.

In all of the experiments, the perturbations to the SST changed the land–sea temperature gradients along the coast. However, these gradients did not affect the storms studied here, because they were too far from the coast. If the storms had traveled closer to the coastline, it is likely that the land–sea contrast created by our SST perturbations would have affected the results. This might also have been the case for a storm that took place in spring, when the land–sea contrast is greater. For our storms, however, the monotonic response to the perturbation amplitude suggests that the storm behavior is realistic, and not the result of unrealistic land–sea baroclinicity, or numerical noise associated with a sudden SST or flux change (as discussed in Semmler et al. 2008).

The difference in the timing of the response of the storms for the two cumulus schemes reflects the different ability of the two schemes to feedback on the vertical motion of the resolved-scale flow. The SST sensitivity time series for the SST-AMP-12km experiments (A1 and A2) in Fig. 4 show the model with the KF cumulus

scheme (A1) responding faster to the SST perturbations. This can also be seen in the storm response in the SST-GRAD-12km experiments (A3 and A4): for KF, the divergence occurs at 0000 UTC 24 February (Fig. 6a), while for BMJ, the divergence starts 3 h later (Fig. 6b). We attribute these differences to the ability of the KF scheme to transmit the activity of its convection back onto the resolved-scale flow [summarized in Gallus (1999), as well as Stensrud (2007, 229–246)]. For these two cumulus schemes, simulation differences are often related to the trigger function (e.g., Baldwin et al. 2002), however, in the FEB2001 storm, both of the schemes activated, so the differences in the trigger functions did not have a strong impact.

6. Conclusions

The sets of simulations analyzed here clarify the role of sea surface temperature (SST) in forcing storm strength during the late stages of development. We were able to separate the competing roles within the WRF model of the cyclogenetic surface fluxes that affect the storm warm sector and the cyclolytic fluxes that damp the storm, by mixing momentum down to the surface or by weakening a storm's low-level temperature gradients. We showed that the surface fluxes under the storm warm sector have a dominant role through their regulation of the heat and moisture in the air that enters the warm conveyor belt (WCB), even after the storm had formed. These results carry the caveat that the response in the model is dependent on the parameterization of the air–sea interaction, and the model behavior in these conditions should be further validated against observations.

The sensitivity analysis metric, $d\mathrm{SLP}(t)/d\mathrm{SST}$, provided a technique for understanding the interplay of the various physical mechanisms associated with the surface forcing of storms. The analysis relies on simple statistics, however, it required that we create unique methods for reducing the storm characteristics to single-variable time series, which we described in section 2c. Additionally, by creating sets of simulations with SST perturbations that were small, large, and in between, we can argue that the storm response was not caused by a boundary or initial condition shock.

Our study offers an explanation for an expanded role of SST in storm forcing; however, the model setup limits the generality of the conclusions. The use of the WRF model provided a simple method for isolating the SST effects, but the upper-level and meridional boundary conditions remained fixed. Thus, our study does not exclude the possibility that, all things being considered, another factor, such as poleward advection of moisture into the WCB or a large-scale adjustment of the troposphere to the changed SST, might be dominant over the surface fluxes, if all variables were allowed to adjust. However, the experimental design allowed us to demonstrate that the surface fluxes under the warm sector create a nonnegligible forcing on storm intensification after the storm has developed.

This research offers some suggestions for future studies. For instance, the interplay of the surface fluxes ahead of the storm warm sector and the fluxes under the warm sector needs further investigation. As a storm progresses along its track, the air that is ingested into the WCB arrives from various locations. Given the results presented here on the surface flux regulation under the warm sector, knowledge of the properties of the air converging into the WCB would allow an improved prediction of late-stage storm intensification. Also, more validation, with observations, of the behavior of the model is needed, particularly over the ocean. The horizontal and temporal resolution of the SST product used for the boundary conditions can be improved, because temporally smoothing SST removes some of its filament structure and this affects the mesoscale response of the storm (Jacobs et al. 2007). Perhaps a similar experiment could be carried out on a recent storm, and the SST could be allowed to evolve in time.

The numerical experiments here suggest that, when considering the role of the ocean in forcing storms that have already started to develop, the absolute values of the SST under the storm need increased attention. In the recent literature, the studies on storms in the Gulf Stream region have focused on the SST forcing associated with temperature gradients (e.g., Semmler et al. 2008; Nakamura and Yamane 2009; Long et al. 2009). Our study suggests the need for a closer look at the role of warm SSTs in storm genesis regions, as well as the role of increased lower-tropospheric moisture, in strengthening storms. Furthermore, the consistent relationship between Q_{VOL} [(2)] and storm strength in our study: increased moisture within the WCB leads to a stronger storm, agrees with the compositing study of Field and Wood (2007). Neither result gives causal proof to stronger storms occurring in a warmer world (e.g., in our study we have fixed the upper-level conditions), but the implications of our study, and that of Field and Wood (2007), are useful to the conversation on theories of midlatitude storm trends in a warming climate.

Acknowledgments. We thank Mark Stoelinga, Nick Bond, Olivier Pauluis, and Rick Steed for useful conversations on this topic. We thank the reviewers and David Schultz for their suggestions, which greatly improved the experimental design and the organization of the paper. This research was sponsored by NASA's

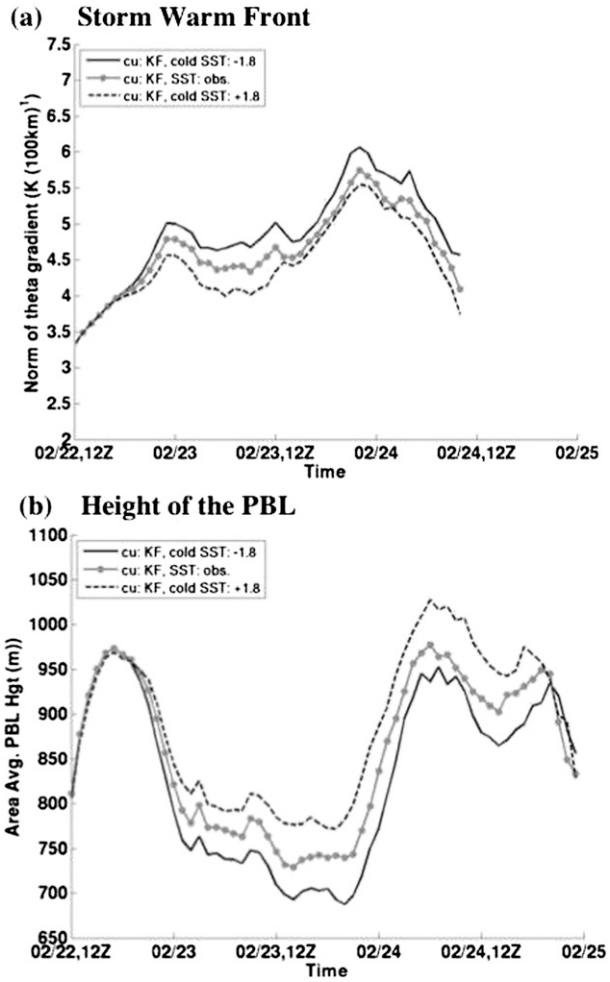

Fig. A1. The times series over the entire integration, including spinup, for the SST-GRAD-12km set of simulations with the KF scheme (experiment A3 in Table 2): (a) the strength of the storm warm front and (b) the height of the PBL. After 0000 UTC 23 Feb, (a) is the same as Fig. 8, and (b) is the same as Fig. 7c.

Ocean Vector Winds Science Team, under Contract 1285662 between the University of Washington and the Jet Propulsion Laboratory.

APPENDIX

Storm Behavior during SST Adjustment

The spinup method we developed for the primary experiments (experiments A1–A4 in Table 2) allows the simulated storm to form without major shocks to the surface fluxes or temperature fronts. As discussed in the methods section, we apply the observed sea surface temperature (SST) for the first 6 h. Over the next 6 h we adjust the SST toward its perturbed state. This creates a smooth adjustment of the simulated atmospheric conditions. Note, however, that this is not the same as using a warm-cycling model.

To determine what influence this adjustment has on the results, we examine the strength of the warm fronts for the SST-GRAD-12km set of simulations with the Kain–Fritsch cumulus scheme (A3) for the entire simulation (Fig. A1a). The strength of the warm fronts for the three experiments diverges between 1800 UTC 22 February and 0000 UTC 23 February, the 6-h period in which the SST is adjusted toward the final perturbed state. Note that Figure A1a from 0000 UTC 23 February onward is the same as Fig. 8. In addition, during the 12-h spinup period, there was no storm, and hence no warm front, and the area determined by the storm warm front at 0000 UTC 23 February is used for area averaging the temperatures. The height of the PBL also demonstrates the slow adjustment during the spinup period (cf. Fig. A1b and Fig. 7c).

REFERENCES

Adamson, D. S., S. E. Belcher, B. J. Hoskins, and R. S. Plant, 2006: Boundary layer friction in midlatitude cyclones. *Quart. J. Roy. Meteor. Soc.,* **132,** 101–124.

Ahmadi-Givi, F., G. C. Graig, and R. S. Plant, 2004: The dynamics of a midlatitude cyclone with very strong latent-heat release. *Quart. J. Roy. Meteor. Soc.,* **130,** 295–323.

Baldwin, M. E., J. S. Kain, and M. P. Kay, 2002: Properties of the convection scheme in NCEP's Eta Model that affect forecast sounding interpretation. *Wea. Forecasting,* **17,** 1063–1079.

Beare, R. J., 2007: Boundary layer mechanisms in extratropical cyclones. *Quart. J. Roy. Meteor. Soc.,* **133,** 503–515.

Betts, A. K., 1986: A new convective adjustment scheme. Part I: Observational and theoretical basis. *Quart. J. Roy. Meteor. Soc.,* **112,** 677–691.

Boutle, I. A., R. J. Beare, S. E. Belcher, and R. S. Plant, 2007: A note on boundary-layer friction in baroclinic cyclones. *Quart. J. Roy. Meteor. Soc.,* **133,** 2137–2141.

——, ——, ——, A. R. Brown, and R. S. Plant, 2010: The moist boundary layer under a mid-latitude weather system. *Bound.-Layer Meteor.,* **134,** 367–386.

——, S. E. Belcher, and R. S. Plant, 2011: Moisture transport in mid-latitude cyclones. *Quart. J. Roy. Meteor. Soc.,* **137,** 360–367.

Brayshaw, D. J., B. Hoskins, and M. Blackburn, 2009: The basic ingredients of the North Atlantic storm track. Part I: Land–sea contrast and orography. *J. Atmos. Sci.,* **66,** 2539–2558.

Brennan, M. J., and G. M. Lackmann, 2005: The influence of incipient latent heat release on the precipitation distribution of the 24–25 January 2000 U.S. East Coast cyclone. *Mon. Wea. Rev.,* **133,** 1913–1937.

Businger, S., T. M. Graziano, M. L. Kaplan, and R. A. Rozumalski, 2005: Cold-air cyclogenesis along the Gulf-Stream front: Investigation of diabatic impacts on cyclone development, frontal structure and track. *Meteor. Atmos. Phys.,* **88,** 65–90.

Cione, J. J., S. Raman, and L. J. Pietrafesa, 1993: The effect of Gulf Stream-induced baroclinicity on the U.S. East Coast winter cyclones. *Mon. Wea. Rev.,* **121,** 421–430.

Davis, C. A., and K. A. Emanuel, 1991: Potential vorticity diagnostics of cyclogenesis. *Mon. Wea. Rev.,* **119,** 1929–1953.

Fantini, M., 1990: The influence of heat and moisture fluxes from the ocean on the development of baroclinic waves. *J. Atmos. Sci.,* **47,** 840–855.

Field, P. R., and R. Wood, 2007: Precipitation and cloud structure in midlatitude clouds. *J. Climate,* **20,** 233–254; Corrigendum, **20,** 5208–5210.

Gallus, W. A., Jr., 1999: Eta simulations of three extreme precipitation events: Sensitivity to resolution and convective parameterization. *Wea. Forecasting.,* **14,** 405–426.

Giordani, H., and G. Caniaux, 2001: Sensitivity of cyclogenesis to sea surface temperature in the northwestern Atlantic. *Mon. Wea. Rev.,* **129,** 1273–1295.

Hakim, G. J., and R. D. Torn, 2008: Ensemble synoptic analysis. *Synoptic–Dynamic Meteorology and Weather Analysis and Forecasting: A Tribute to Fred Sanders, Meteor. Monogr.,* No. 55, Amer. Meteor. Soc., 147–161.

Hewson, T. D., 1998: Objective fronts. *Meteor. Appl.,* **5,** 37–65.

Hong, S.-Y., Y. Noh, and J. Dudhia, 2006: A new vertical diffusion package with an explicit treatment of entrainment processes. *Mon. Wea. Rev.,* **134,** 2318–2341.

Hoskins, B. J., and K. Hodges, 2002: New perspectives on the Northern Hemisphere winter storm tracks. *J. Atmos. Sci.,* **59,** 1041–1061.

Jacobs, N. A., G. M. Lackmann, and S. Raman, 2005: The combined effects of Gulf Stream–induced baroclinicity and upper-level vorticity on U.S. East Coast extratropical cyclones. *Mon. Wea. Rev.,* **133,** 2494–2501.

——, S. Raman, G. M. Lackmann, and P. P. Childs Jr., 2007: The influence of the Gulf Stream induced SST gradients on the U.S. East Coast winter storm of 24–25 January 2000. *Int. J. Remote Sens.,* **29,** 6145–6174.

Janjic, Z. I., 1994: The step-mountain eta coordinate model: Further developments of the convection, viscous sublayer, and turbulence closure schemes. *Mon. Wea. Rev.,* **122,** 927–945.

Jung, T., and F. Vitart, 2006: Short-range and medium-range weather forecasting in the extratropics during wintertime with and without an interactive ocean. *Mon. Wea. Rev.,* **134,** 1972–1986.

Kain, J. S., and J. M. Fritsch, 1993: Convective parameterization for mesoscale models: The Kain–Fritsch scheme. *The Representation of Cumulus Convection in Numerical Models, Meteor. Monogr.,* No. 24, Amer. Meteor. Soc., 165–170.

Kelly, K. A., R. J. Small, R. M. Samelson, B. Qiu, T. M. Joyce, Y.-O. Kwon, and M. F. Cronin, 2010: Western boundary currents and frontal air–sea interaction: Gulf Stream and Kuroshio Extension. *J. Climate,* **23,** 5644–5667.

Kiehl, J. T., J. J. Hack, G. B. Bonan, B. A. Boville, B. P. Briegleb, D. L. Williamson, and P. J. Rasch, 1996: Description of the NCAR Community Climate Model (CCM3). NCAR Tech. Note NCAR/TN-4201-STR, 152 pp.

Kuo, Y.-H., R. Reed, and S. Low-Nam, 1991: Effects of surface energy fluxes during the early development and rapid intensification stages of seven explosive cyclones in the western Atlantic. *Mon. Wea. Rev.,* **119,** 457–476.

——, ——, and Y. Lio, 1996: The ERICA IOP5 storm. Part III: Mesoscale cyclogenesis and precipitation parameterization. *Mon. Wea. Rev.,* **124,** 1409–1434.

Long, Z., W. Perrie, J. Gyakum, R. Laprise, and D. Caya, 2009: Scenario changes in the climatology of winter midlatitude cyclone activity over eastern North America and the Northwest Atlantic. *J. Geophys. Res.,* **114,** D12111, doi:10.1029/2008JD010869.

Martin, J. E., 2006: *Mid-Latitude Atmospheric Dynamics*. Wiley, 336 pp.

Minobe, S., A. Kuwano-Yoshida, N. Komori, S. P. Xie, and R. J. Small, 2008: Influence of the Gulf Stream on the troposphere. *Nature,* **452,** 206–210.

Nakamura, H., T. Sampe, Y. Tanimoto, and A. Shimpo, 2004: Observed associations among storm tracks, jet streams and midlatitude oceanic fronts. *Earth's Climate: The Ocean–Atmosphere Interaction, Geophys. Monogr.,* Vol. 147, Amer. Geophys. Union, 329–345.

Nakamura, M., and S. Yamane, 2009: Dominant anomaly patterns in the near-surface baroclinicity and accompanying anomalies in the atmosphere and oceans. Part I: North Atlantic basin. *J. Climate,* **22,** 880–904.

Petterssen, S., and S. J. Smebye, 1971: On the development of extratropical cyclones. *Quart. J. Roy. Meteor. Soc.,* **97,** 457–482.

Plant, R. S., G. C. Craig, and S. L. Gray, 2003: On a threefold classification of extratropical cyclogenesis. *Quart. J. Roy. Meteor. Soc.,* **129,** 2989–3012.

Pomroy, H. R., and A. J. Thorpe, 2000: The evolution and dynamical role of reduced upper-tropospheric potential vorticity in Intense Observing Period One of FASTEX. *Mon. Wea. Rev.,* **128,** 1817–1834.

Posselt, D. J., and J. E. Martin, 2004: The effect of latent heat release on the evolution of a warm occluded thermal structure. *Mon. Wea. Rev.,* **132,** 578–599.

Reed, R. J., G. Grell, and Y.-H. Kuo, 1993a: The ERICA IOP 5 storm. Part I: Analysis and simulation. *Mon. Wea. Rev.,* **121,** 1577–1594.

——, ——, and ——, 1993b: The ERICA IOP 5 storm. Part II: Sensitivity tests and further diagnosis based on model output. *Mon. Wea. Rev.,* **121,** 1595–1612.

Reynolds, R. W., and T. M. Smith, 1995: A high-resolution global sea surface temperature climatology. *J. Climate,* **8,** 1571–1583.

——, N. A. Rayner, T. M. Smith, D. C. Stokes, and W. Wang, 2002: An improved in situ and satellite SST analysis for climate. *J. Climate,* **15,** 1609–1625.

Sanders, F., and J. R. Gyakum, 1980: Synoptic-dynamic climatology of the "bomb." *Mon. Wea. Rev.,* **108,** 1589–1606.

Semmler, T., S. Varghese, R. McGrath, P. Nolan, S. Wang, P. Lynch, and C. O'Dowd, 2008: Regional model simulation of North Atlantic cyclones: Present climate and idealized response to increase sea surface temperature. *J. Geophys. Res.,* **113,** D02107, doi:10.1029/2006JD008213.

Shaman, J., R. M. Samelson, and E. Skyllingstad, 2010: Air–sea fluxes over the Gulf Stream region: Atmospheric controls and trends. *J. Climate,* **23,** 2651–2670.

Sinclair, V. A., S. L. Gray, and S. E. Belcher, 2008: Boundary-layer ventilation by baroclinic life cycles. *Quart. J. Roy. Meteor. Soc.,* **134,** 1409–1424.

Skamarock, W. C., and Coauthors, 2008: A description of the advanced research WRF version 3. NCAR Tech. Note NCAR/TN-475+STR, 125 pp. [Available online at http://www.mmm.ucar.edu/wrf/users/docs/arw_v3.pdf.]

Stensrud, D. J., 2007: *Parameterization Schemes: Keys to Understanding Numerical Weather Prediction Models*. Cambridge University Press, 478 pp.

Stoelinga, M. T., 1996: A potential vorticity–based study on the role of diabatic heating and friction in a numerically

simulated baroclinic cyclone. *Mon. Wea. Rev.,* **124,** 849–874.

——, 2003: Comments on "The evolution and dynamical role of reduced upper-tropospheric potential vorticity in Intensive Observing Period One of FASTEX." *Mon. Wea. Rev.,* **131,** 1944–1947.

Thompson, G., R. M. Rasmussen, and K. Manning, 2004: Explicit forecasts of winter precipitation using an improved bulk microphysics scheme. Part I: Description and sensitivity analysis. *Mon. Wea. Rev.,* **132,** 519–542.

Uppala, S. M., and Coauthors, 2005: The ERA-40 Re-Analysis. *Quart. J. Roy. Meteor. Soc.,* **131,** 2961–3012.

Vukovich, F. M., J. W. Dunn, and B. W. Crissman, 1991: Aspects of the evolution of the marine boundary layer during the cold-air outbreaks off the southeast coast of the United States. *Mon. Wea. Rev.,* **119,** 2252–2278.

Wernli, H., and H. C. Davies, 1997: A Lagrangian based analysis of extratropical cyclones: The method and some applications. *Quart. J. Roy. Meteor. Soc.,* **123,** 467–490.